NANO LETTERS

pubs.acs.org/NanoLett

Electric Field Control of Spin Rotation in Bilayer Graphene

Paolo Michetti,*,† Patrik Recher,*,† and Giuseppe Iannaccone*,‡

†Institute for Theoretical Physics and Astrophysics, University of Würzburg, D-97074 Würzburg, Germany, and ‡Dipartimento di Ingegneria dell'Informazione: Elettronica, Informatica, Telecomunicazioni, Università di Pisa, Via Caruso 16, 56122 Pisa, Italy

ABSTRACT The manipulation of the electron spin degree of freedom is at the core of the spintronics paradigm, which offers the perspective of reduced power consumption, enabled by the decoupling of information processing from net charge transfer. Spintronics also offers the possibility of devising hybrid devices able to perform logic, communication, and storage operations. Graphene, with its potentially long spin-coherence length, is a promising material for spin-encoded information transport. However, the small spin−orbit interaction is also a limitation for the design of conventional devices based on the canonical Datta-Das spin field-effect transistors. An alternative solution can be found in magnetic doping of graphene or, as discussed in the present work, in exploiting the proximity effect between graphene and ferromagnetic oxides (FOs). Graphene in proximity to FO experiences an exchange proximity interaction, that acts as an effective Zeeman field for electrons in graphene, inducing a spin precession around the magnetization axis of the FO. Here we show that in an appropriately designed double-gate field-effect transistor, with a bilayer graphene channel and FO used as a gate dielectric, spin-precession of carriers can be turned ON and OFF with the application of a differential voltage to the gates. This feature is directly probed in the spin-resolved conductance of the bilayer.

KEYWORDS Graphene bilayer, spintronics, spin FET, spin precession, spin dependent transport, exchange proximity interaction

Graphene has attracted much attention since its first experimental fabrication,[1] due to its exceptional electronic properties linked to the Dirac physics of its low-energy quasi-particles.[2] Thanks to its extremely high mobility,[3] graphene is also a promising material for nanoelectronics, where however the presence of a semiconducting gap is required. One-dimensional graphene-related structures like nanoribbons[4] and carbon nanotubes[5] have been employed successfully for nanoelectronic devices, but their practical applications are limited by the need of single-atom precision in the definition of their transversal width and radius, respectively. Carbon-based materials like epitaxial graphene on SiC[6] and bilayer graphene[7] have been shown to be promising for the realization of tunneling field-effect transistors (FETs), while the gap is not sufficient for conventional FETs.[8,9]

Spin−orbit coupling plays a crucial role in spintronics, providing a way to manipulate electron spin by means of an external field. This is at the heart of most of proposed spintronic devices, such as the Datta-Das spin-FET.[10] However, theoretical studies have shown that spin−orbit coupling in graphene is extremely small.[11,12] Therefore, conventional spintronics mechanisms are not applicable to graphene. On the other hand, graphene is attractive for spintronics because of its long spin-coherence time.[13] Moreover, simulations show that magnetic doping[14] in graphene, or edge functionalization in GNRs,[15,16] lead to spin-splitted bands and potentially to a semimetal dispersion relation, particularly attractive for spintronic applications.[17]

An alternative approach can come from the exploitation of the interfacial proximity with a ferromagnetic oxide (FO). Indeeed, it has been proposed that a spin splitting (acting as an effective Zeeman field) can arise in graphene due to exchange proximity interaction (EPI) between electrons in graphene and localized electrons in a FO layer adjacent to the graphene layer.[18,19] The effective Zeeman splitting (which has been estimated to be of the order of 5 meV[19]) acts on the spin of graphene carriers inducing a precession around the magnetization axis of the FO. The same mechanism was proposed for bilayer graphene, and the modification of the electronic structure and of the magnetoresistance as a function of relative angle between the magnetization axes of the upper and lower FO spacers has been investigated.[20] The spin filtering properties of bilayer graphene with multiple *magnetic* barriers with EPI were also investigated in ref.[21] However, the control on the spin-transport properties exerted by an electric field, driven by gates, has not yet been the subject of investigation.

It is possible to induce an energy gap in bilayer graphene by applying an electric field perpendicular to the graphene plane.[22−25] For small kinetic energy, first valence and conduction band wave functions are driven toward different planes of the bilayer by the applied field. This means that electrons in the first valence and conduction band have different probabilities to be found on the upper and lower plane. Therefore, we can devise a way to tune the spin-rotation of carriers in the bilayer graphene by reversing the gate voltage.

* To whom correspondence should be addressed: michetti@physik.uni-wuerzburg.de, precher@physik.uni-wuerzburg.de, g.iannaccone@iet.unipi.it.
Received for review: 07/1/2010
Published on Web: 10/07/2010

DOI: 10.1021/nl102298n | *Nano Lett.* **2010,** *10,* 4463–4469

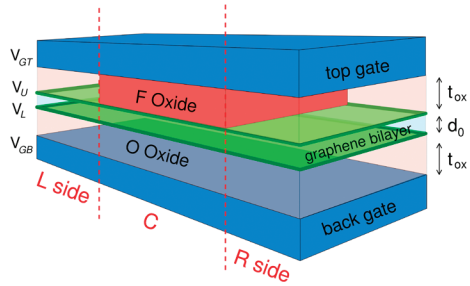

FIGURE 1. Picture representing a double-gated graphene bilayer structure in which the central part (C) is characterized by the use of a ferromagnetic oxide as spacer between the upper layer and the top gate. The oxide thickness t_{ox} and the interlayer distance d_0 are indicated. The potential of the top gate V_{GT} and the one of the back gate V_{GB} are externally fixed, inducing potential values V_U and V_L on the upper and lower graphene layer, respectively, via nonlinear Poisson equation.

We consider a double gate bilayer graphene FET where a FO is used as the insulating layer between the bilayer graphene channel and the top gate, while an ordinary oxide (OO) is used as insulating layer for the bottom gate, as shown in Figure 1. EPI interaction will mainly affect electrons on the upper graphene layer. By applying a *direct* or *inverse* differential voltage between the gates, we determine whether conduction electrons do or do not feel the EPI interaction, and accordingly the associated wave functions are quasi-localized on the upper or on the lower plane. Consequently, we are able to switch on or off spin precession.

Model. We discuss here in very generic terms the difference between an insulating material made of an ordinary oxide and of a FO. In both materials electrons reside in similarly localized wave functions, as is proper for an insulating material, but in a FO they will be also characterized by a majority spin component. If we place a graphene sheet in proximity to a FO, rather than to a OO, in general we can expect a similar contribution for the direct Coulomb interaction between electrons in graphene and in the oxide, but a completely different contribution from the exchange interaction. Indeed, the exchange interaction requires "exchanged" electrons to have the same spin orientation, and therefore graphene electrons will feel a very different effective EPI for majority and minority spin components with respect to the FO. Moreover, while the direct Coulomb interaction is long ranged, EPI requires an overlap of the wave functions of "exchanged" particles. For this reason EPI interaction, as pointed out in ref 20, is essentially limited to the graphene layer placed in direct proximity to the FO, and it is negligible on more distant layers.

We assume here the simplest situation, in which a thin FO layer is deposited between the upper graphene plane and the top gate, with magnetization $\vec{M}$, and an OO layer is instead used as insulator between the lower graphene layer and the back gate (Figure 1). The electronic states of bilayer graphene can be described, near the K point, by the following Hamiltonian[26]

$$H = H_0 + H_m = U_0\mathbb{I} + \begin{pmatrix} \frac{\Delta}{2} + h_m & \hat{\pi} & t_\perp & 0 \\ \hat{\pi}^\dagger & \frac{\Delta}{2} + h_m & 0 & 0 \\ t_\perp & 0 & -\frac{\Delta}{2} & \hat{\pi}^\dagger \\ 0 & 0 & \hat{\pi} & -\frac{\Delta}{2} \end{pmatrix} \tag{1}$$

where $U_0 = -q(V_U + V_L)/2$ and $\Delta = -q(V_U - V_L)$, with V_U and V_L the upper and lower layer potential, respectively, and q is the value of the absolute elementary charge. In the following, let us denote with the index U the variables relating to the upper (U) layer, and with the index L those relating to the lower (L) layer. $\hat{\pi} = v_F(p_x + ip_y)$ is the kinetic energy operator (with $p_y \rightarrow -p_y$ for the K' valley), h_m is an effective energy term due to the EPI with the ferromagnetic insulators. We use the parameters $t_\perp = 0.39$ eV,[27,28] i.e., the bilayer interplane coupling, and $v_f \approx 10^6$ m/s.[29] Other interlayer coupling terms are neglected, in the spirit of refs 19, 20, and 29, as they would not change the qualitative features of the phenomenon described in this work. The Hamiltonian acts on wave functions of the form

$$\Psi = \begin{pmatrix} \chi_A \\ \chi_B \\ \chi_{B'} \\ \chi_{A'} \end{pmatrix} \frac{e^{ik_x x} e^{ik_y y}}{\sqrt{L_x L_y}} \tag{2}$$

where A, B refer to the two inequivalent carbon atoms on the upper graphene layer, A′, B′ to that of the lower layer. L_x and L_y are the channel dimensions along X and Y directions. Now we distinguish the two spin components along the Z axis, perpendicular to the plane; therefore χ_X, with X = A, B, A′, B′, has to be regarded as a two-component spinor

$$\chi_X = \begin{pmatrix} \phi_{X\uparrow} \\ \phi_{X\downarrow} \end{pmatrix} \tag{3}$$

The elements V_U, V_L, π, and $t_\perp$ are diagonal in the spinor space, while off-diagonal terms can be due to the presence of an effective Zeeman field. If we imagine to put the upper graphene layer in contact with a ferromagnetic insulator having a polarization on the XY plane, the exchange interaction gives rise to an off-diagonal coupling in the spinor space of the kind

$$h_m = \alpha\vec{M}\vec{S} = \frac{E_Z}{2}\begin{pmatrix} 0 & m_x - im_y \\ m_x + im_y & 0 \end{pmatrix} \tag{4}$$

DOI: 10.1021/nl102298n | *Nano Lett.* **2010,** *10,* 4463–4469

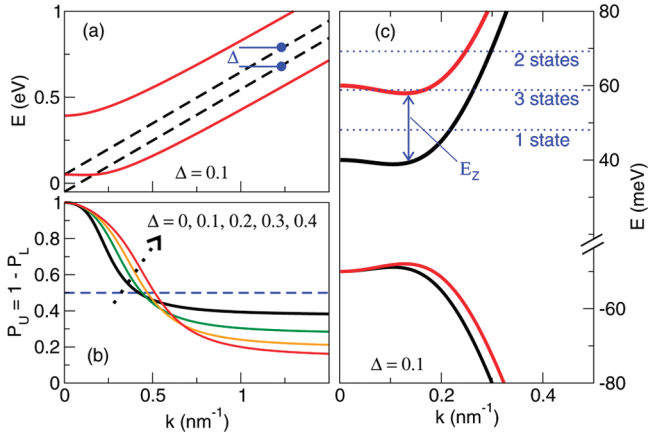

FIGURE 2. (a) Bilayer dispersion curves (solid lines) compared with the Dirac dispersion curves for the upper and lower graphene planes without interplane mixing interaction (dashed line), for $V_U = 0.05$ eV and $V_L = -0.05$ eV ($\Delta = 0.1$ eV). (b) Projection of the conduction band states onto the upper plane as a function of k, for increasing Δ. The black solid line corresponds to the case in (a). (c) Dispersion curve for a bilayer system with EPI interaction on the upper plane with $E_Z = 20$ meV.

where $\hat{M} = (m_x, m_y)$ is the versor of the magnetization vector $\vec{M}$. For simplicity, we assume for the upper layer a similar effective Zeeman coupling h_m for the A and B sites, while EPI vanishes on the lower plane sites A′ and B′.

Bilayer Graphene. The idea of controlling spin rotation of bilayer graphene is essentially based on the plane-localization properties of the bilayer spinors, when a vertical field is applied. In particular, let us assume for a moment no EPI interaction, i.e., $\alpha = 0$ ($H = H_0$). In this case the eigenvalues near the K, or K', point, are given by the formula[26]

$$(E_\eta)^\pm = V_0 \pm \sqrt{\frac{\Delta^2}{4} + \hbar v_f k^2 + \frac{t_\perp^2}{2} + \eta t_\perp \sqrt{\frac{t_\perp^2}{4} + \left(\frac{\Delta^2}{t_\perp^2} + 1\right)\hbar^2 v_f^2 k^2}} \tag{5}$$

with $\eta = \pm 1$ for the first ($\eta = -1$) and second ($\eta = +1$) conduction (+) or valence (−) band. The bilayer spinors, for a given $\vec{k}$ and energy E, are obtained by solving the linear system $(H_0 - E)\Psi = 0$. In Figure 2a we show the bilayer dispersion curve, compared with the graphene dispersion curves

$$E_+^\pm = \pm\hbar v_f k + \frac{\Delta}{2}$$

and

$$E_-^\pm = \pm\hbar v_f k - \frac{\Delta}{2}$$

obtained from eq 5 by decoupling the two layers ($t_\perp = 0$).

In Figure 2b we plot the projection of the first bilayer conduction band states ($P_U = |\chi_A|^2 + |\chi_B|^2$) on the U plane. The behavior of the projection on the U plane can be easily understood from the bilayer dispersion curve. In fact, at $k = 0$, states of the first bilayer conduction band stand on the Dirac point of the U graphene layer. At $k = 0$, the A and B sublattices are not coupled by the kinetic term $\hat{\pi}$ in the Hamiltonian in eq 1, therefore B and A′ sublattices are not mixed by $t_\perp$ and retain their original character. Correspondingly, the spinor of the first conduction band will have a 100% weight on the B sublattice. With increasing k, the bilayer spinors have mixed contributions from the two planes and, eventually, at sufficiently large k, P_U tends to a constant value. An explanation for this comes from the fact that for large k, the bilayer conduction bands essentially originate from the mixing of only the n-type part of the Dirac cones for the U and L graphene sheets (shown in Figure 2a), while contributions from the p-like part may be neglected. This leads to a two-level system with a fixed energy separation of Δ, as plotted in Figure 2a, and fixed tunnel-coupling $t_\perp/2$. The solutions of the two level system are

$$E_\pm = \hbar v_f k \pm \sqrt{\frac{\Delta^2}{4} + \frac{t_\perp^2}{4}}$$

which correspond to the asymptotic behavior of bilayer conduction bands for large k and

$$P_U = \frac{1}{1 + \left(\frac{\Delta}{t_\perp} - \sqrt{1 + \frac{\Delta^2}{t_\perp^2}}\right)^2} \tag{6}$$

for the first conduction band ($\eta = -1$), which explains the plateau in Figure 2b at large k. We note that, for a given k, P_U of the first conduction band corresponds to P_L of the first valence band, and by reversing the potential of both layers one would perfectly exchange the projection properties of the two bands.

In Figure 2c, we plot the first conduction and valence band of a bilayer graphene subjected to EPI interaction as described by the Hamiltonian eq 1, with $E_Z = 20$ meV, and an interlayer energy difference of $\Delta = 0.1$ eV. When the EPI interaction is taken into account, electronic wavefuctions traveling on the U plane are subject to an effective Zeeman interaction, basically proportional to P_U, that results in a spin splitting of the bilayer bands by $P_U E_Z$. If we reverse Δ, which can be realized by inverting the bias of top and back gates, the spin splitting of conduction and valence bands is inverted, as well as $P_U \leftrightarrow P_L$, and the Zeeman splitting at small k will vanish in the conduction band. In a regime in which small k states are responsible for transport through a FO-contacted bilayer region, we will therefore have a degree of control over the electron spin rotation induced by the effective Zeeman field.

DOI: 10.1021/nl102298n | Nano Lett. 2010, 10, 4463–4469

Transmission through a FO Gated Region. To calculate the spin rotation properties of our system, we analyze the transmission through a region of the bilayer in which the EPI coupling is active, as is the case in Figure 1. For simplicity, we imagine abrupt boundary conditions such that the contact with the FO is limited to the upper plane of the graphene bilayer from $x = 0$ to $x = L_c$. We consider an incoming conduction band electron from the left side (LS) ($x < 0$) of given $\vec{k}$ and therefore energy E_k, with a chosen ↑ spin polarization. Elastic transmission through the active EPI zone conserves k_y, because of the space homogeneity along the Y axis, but not the spin, and leads to reflected and transmitted components to the left and right sides (RS), respectively (of ↑ and ↓ spin character).

In particular, the LS and RS are described by the Hamiltonian eq 1, with $E_Z = 0$. We can find, disregarding the spin which is here conserved, four possible values of the wavevector k_x compatible with k_y and energy E: k_x and $-k_x$, which are propagating modes, $\tilde{k}_x$ and $-\tilde{k}_x$, which can correspond alternatively to propagating modes or to evanescent modes, with a finite imaginary part.[29] The number of propagating modes (with real wavevector) corresponds to the number of intersection points of the conduction bands with the horizontal line $E = E_k$ in Figure 2a. The remaining modes are evanescent. Therefore the total wave functions on the LS and RS can be written as

$$\Psi_{\mathrm{L}}(0) = \mathbb{C}_{\mathrm{L}}\vec{r} + \mathbb{C}_{\mathrm{IN}}\vec{s} \tag{7}$$

$$\Psi_{\mathrm{C}}(L) = \mathbb{C}_{\mathrm{R}}\vec{t} \tag{8}$$

where the matrices $\mathbb{C}_{\mathrm{L}}$, $\mathbb{C}_{\mathrm{R}}$, and $\mathbb{C}_{\mathrm{IN}}$ are built from the spinor set of the bilayer system in eq 1 without EPI. $\vec{s}$ is the vector describing the spin polarization with respect to the Z axis of the incoming particle. Our calculation starts from fully polarized incoming particles, for which $\vec{s} = (1, 0)^T$. For all matrices, rows run over the sublattices $\{i = \mathrm{A}\uparrow, \mathrm{A}\downarrow, \mathrm{B}\uparrow, \mathrm{B}\downarrow, \mathrm{A}'\uparrow, \mathrm{A}'\downarrow, \mathrm{B}'\uparrow, \mathrm{B}'\downarrow\}$, while columns run over the left region output modes $\{j = -k_x\uparrow, -k_x\downarrow, -\tilde{k}_x\uparrow, -\tilde{k}_x\downarrow\}$ for $\mathbb{C}_{\mathrm{L}}$, right region output modes $\{j = k_x\uparrow, k_x\downarrow, \tilde{k}_x\uparrow, \tilde{k}_x\downarrow\}$ for $\mathbb{C}_{\mathrm{R}}$, and incoming modes $\{j = k_x\uparrow, k_x\downarrow\}$ for $\mathbb{C}_{\mathrm{IN}}$. The output coefficients are collected in

$$\vec{r} = (r_1, r_{-1}, \tilde{r}_1, \tilde{r}_{-1})^T \tag{9}$$

$$\vec{t} = (t_1, t_{-1}, \tilde{t}_1, \tilde{t}_{-1})^T \tag{10}$$

with the tunneling coefficients t_1, t_{-1}, $\tilde{t}_1$, $\tilde{t}_{-1}$ for allowed modes in up or down spin orientation, and the reflection coefficients defined in a similar manner as r_1, r_{-1}, $\tilde{r}_1$, and $\tilde{r}_{-1}$.

In the central part of the system we have a mixing of spin components induced by the effective Zeeman splitting. Solving the secular equation for the Hamiltonian in eq 1 for a given energy E and in-plane momentum k_y, we obtain eight solutions for the wavevector $k_x = \alpha_n$ with $n = 1, 2, \ldots, 8$. The corresponding modes are described by the spinor $\Psi_{\alpha_n}{}^M$ where the M index is used to specify that these states are for the system with Zeeman interaction. The scattering state in the central part of the system can be generally expressed as

$$\Psi_{\mathrm{C}} = \sum_n a_n \Psi_{\alpha_n}{}^M = \mathbb{C}_{\mathrm{C}}\vec{a} \tag{11}$$

The Dirac equation requires the continuity of spinors at the boundary $x = 0$ and $x = L$, which is now expressed by the following linear relations

$$\mathbb{C}_{\mathrm{C}}\vec{a} = \mathbb{C}_{\mathrm{L}}\vec{r} + \mathbb{C}_{\mathrm{IN}}\vec{s} \tag{12}$$

$$\mathbb{C}_{\mathrm{R}}\vec{t} = \mathbb{C}_{\mathrm{C}}\mathbb{P}\vec{a} \tag{13}$$

with $\mathbb{P}$ describing the phase accumulation of the different components of the scattering state by traveling through the C region. After elimination of $\vec{a}$, the problem is reduced to the solution of a linear system of the kind $\mathbb{M}x = \vec{S}$, with

$$\vec{x} = \begin{pmatrix} \vec{t} \\ \vec{r} \end{pmatrix}$$

which can be easily solved by standard numerical techniques. In practice, a source term $\vec{S}$, describing the incoming particle, pumps the linear system described through the dynamical matrix $\mathbb{M}$, which carries all the information about the transmission through the central region and determines the output steady state described by $\vec{x}$.

We consider the transmission of our system, which is given by the sum of the outgoing propagating components in the RS. We choose FO with magnetization along Y, so that in the C region we have spin-splitted bands (Y-SSB), eigenstates of S_y, while we inject and detect in the LS and RS electron spin-polarized along Z. Note that as explained before, with *direct* gate bias, the conduction bands will be spin-splitted, while for a *reverse* bias the spin splitting is negligible. In Figure 3, we show the spin differential transmission $T_s = T_{\uparrow\uparrow} - T_{\uparrow\downarrow}$ through the central region with FO deposited on the U layer, with $E_Z = 20$ meV and $L_C = 150a_{C-C}$. T_s is calculated as a function of the wavevector of the incoming particle in the LS. Figure 3a is calculated with

DOI: 10.1021/nl102298n | *Nano Lett.* **2010,** *10,* 4463–4469

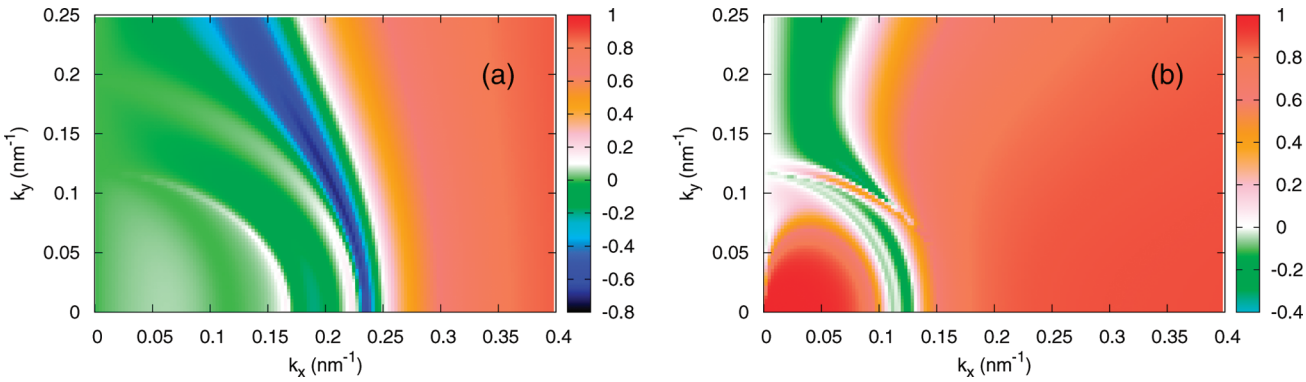

FIGURE 3. (a) Spin differential transmission $T_s = T_{\uparrow\uparrow} - T_{\uparrow\downarrow}$ through the C region of $L_C = 150a_{C-C}$ with EPI and $\Delta = 0.1$ eV, as a function of the wavevector of the incoming particle. (b) T_s for a *reverse* potential energy difference of $\Delta = -0.1$ eV.

a *direct* potential energy difference between the graphene planes of $\Delta = 0.1$ eV. Indeed a marked resonance is observed with negative values of T_s. Electrons of this wavevector are transmitted through the barrier with a spin rotation of π. In Figure 3b, where $\Delta = -0.1$ eV is *reversed*, such a feature is absent and electrons preferentially preserve their spin orientation. The spin-transmission properties are therefore dramatically affected by changing between *direct* and *reverse* bias of the top and back gates.

In particular this resonance falls into the Mexican hat region of the upper Y-SSB (Figure 2c), where three propagating states are active: two from the upper Y-SSB and one from the lower one. The resonance condition is given by the existence of two propagating modes, one from each of the two Y-SSBs, for which $\Delta k_x L_c = \pi + 2n\pi$, with $n = 0, 1, \ldots$ (here $n = 0$ applies). In fact, an incoming particle, spin-polarized along Z, can be transmitted in the C region as a linear combination of two states from the two bands (eigenstates of S_y). These components, traveling through the C region, acquire a phase difference of π, which corresponds to a net spin-flip process. Note that the Mexican hat-like dispersion makes it possible to have two propagating states with large Δk_x, allowing the fulfillment of the resonance condition with L_C as small as 20 nm. Of course, choosing different values for L_c leads to different positions of the spin-flip transmission resonance.

For an incoming particle of lower energy, only the lower Y-SSB contributes propagating components in the C region as shown in Figure 2c. The overall transmission probability $T = T_{\uparrow\uparrow} + T_{\uparrow\downarrow}$ has an upper limit of 0.5, because the propagating component is an eigenstate of S_y and can be seen as a combination of half and half S_z spin components. For the same reason, the spin differential transmission is close to zero. For an incoming particle of energy above the resonance, instead, there is one propagating component for each of the Y-SSBs (see Figure 2c). However Δk_x between these components is much smaller with respect to the resonance case and their phase difference accumulated by traveling through the C region is negligible. Therefore both the spin differential transmission and the overall transmission are close to unity.

Conductance. A readily measurable property of the system is its conductance. We have therefore calculated the 2D conductance of the proposed device. In particular we are interested in the spin-flipped relative conductance $X_s = G_{\uparrow\downarrow}/G$, with $G = G_{\uparrow\downarrow} + G_{\uparrow\uparrow}$, which is a measure of the efficiency of spin control. The 2D two-terminal conductance, which is defined by $dI_x = G_x dV_{DS}$, is expressed as

$$G_x = \frac{gq^2}{(2\pi)^2} \int_{BZ} dk_x\, dk_y T_{k_x,k_y} v_x \frac{df(E_{k_x,k_y} - \mu)}{dE} \qquad (14)$$

with $g = 4$ (accounting for the valley and spin degeneracy), v_x the group velocity along the transport direction, $f(E)$ the Fermi−Dirac distribution function, and μ the electrochemical potential. Integration is performed over the Brillouin zone.

In Figure 4 we show the spin-flip relative conductance X_s as a function of the electrochemical potential for L_C from $50a_{C-C}$ to $200a_{C-C}$, at a temperature of 1.8 K. Figure 4a is computed with a *direct* gate bias of $\Delta = 0.1$ eV, while Figure 4b shows the case with the *reverse* bias. The resonance present in panel a, corresponding to an electrochemical potential for which the spin-flip affects more than 80% of transmitted electrons, is completely absent in panel b, where electrons tend to preserve their original spin. This calculation clearly demonstrates that we are able to control the spin-flip of carriers traveling through the system by changing the gate bias.

The total conductance is thermally activated as μ approaches the bottom of the conduction band of the LS region. As μ enters the three-states spectral region in Figure 2c the conductance spin properties are dominated by the behavior of the transmission probability in Figure 3a. This leads, with a *direct* bias, to a pronounced resonance of X_s. A fundamental factor for the appearance of this resonance is that the spin differential transmission resonance in Figure 3a is almost isotropic for small k_y, similar to the LS dispersion curve, deviating only for large k_y. Therefore, it is possible, with the appropriate electrochemical potential, to adjust the

DOI: 10.1021/nl102298n | *Nano Lett.* **2010,** *10,* 4463–4469

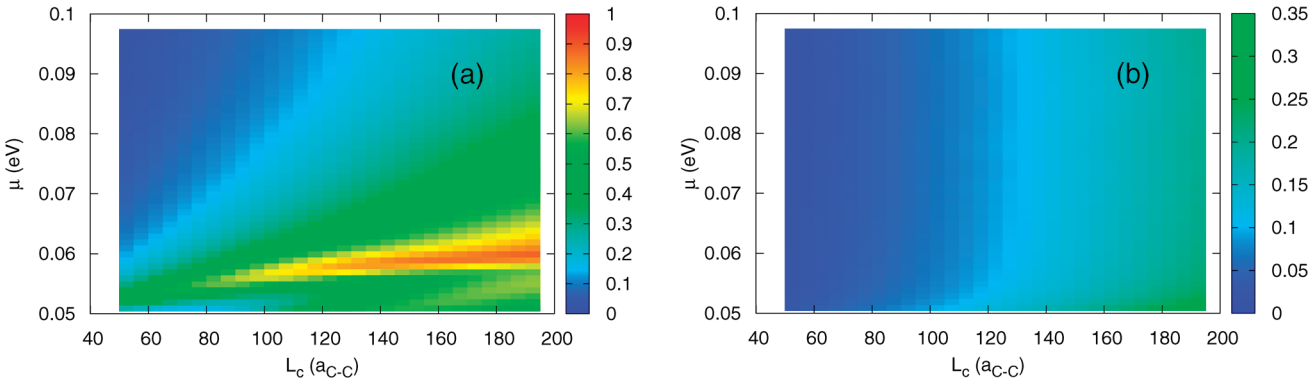

FIGURE 4. (a) Spin-flip relative conductance X_s, at $T = 1.8$ K, for a system with *direct* bias of $\Delta = 0.1$ eV, and *inverse* bias (b) at $T = 1.8$ K. μ refers to the electrochemical potential with respect to midgap of the bilayer bands, as shown in Figure 2c.

Fermi level to this transmission resonance. The states relevant to the conductance will therefore be quite well collimated on the spin-flip transmission resonance. As expected, an increase of the temperature leads to a broader state population, gradually blurring away this feature.

Self-Consistent Analysis. To provide an indication of the real control that the gates exert on the system, and therefore of the observability of the phenomenon, we performed a self-consistent electrostatic analysis. Indeed, we can fix the absolute value of the chemical potential, but we cannot set the difference between the electrochemical potential and the bilayer graphene midgap. In other words, the value of the potential of the U and L layers of the graphene bilayer is the result of the self-consistent calculation, which depends on the gate voltages, taking into account the capacitive coupling with the gates. In a double gate FET we can independently fix the top and back gate voltages (V_{GT} and V_{GB}). Alternatively we can give the average gate potential

$$V_{Gm} = \frac{V_{GT} + V_{GB}}{2}$$

which is responsible for rigidly shifting the bands (and therefore varying the electrochemical potential μ with respect to midgap), and the gate voltage difference $\Delta V_G = V_{GB} - V_{GT}$ which opens up the semiconducting gap of the graphene bilayer. To describe the electrostatics of the system, we apply to the graphene bilayer the plane capacitor model described in refs 8 and 30 Another way to describe the charge on the U and L plane is band filling. In fact, the occupation of each one of the graphene bilayer states is described by the Fermi−Dirac distribution, and the charge it carries can be distributed on the U and L plane according to P_U and P_L. The two descriptions of the system, electrostatics and statistics, should be consistent and their simultaneous solution fixes the U and L potentials and, therefore, μ.

We focus our calculation on a system with $\Delta \approx 0.1$ eV, and analyze the control on the electrochemical potential with respect to the midgap of the graphene bilayer. In Figure 5, we show μ as a function of the average gate potential V_{Gm}, where a potential difference $V_{GB} - V_{GT} = 0.023$ and 0.034 V has been applied for $t_{ox} = 1$ and 2 nm, respectively (values

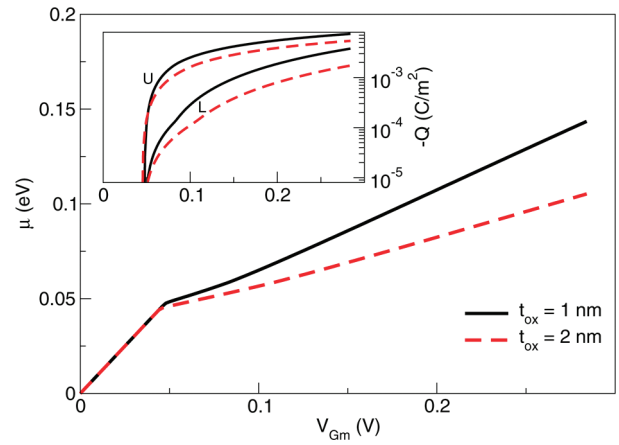

FIGURE 5. Electrochemical potential as a function of V_{Gm} for a double gate graphene bilayer in quasi-equilibrium condition, at a temperature $T = 1.8$ K, calculated for $t_{ox} = 1$, $\Delta V_G = 0.023$ V and $t_{ox} = 2$ nm, $\Delta V_G = 0.034$ V. In the inset the charge accumulated on the U and L graphene layers in the two cases is shown.

which lead to $V_L - V_U \approx 0.1$ V). When the device is empty, the electrochemical potential linearly increases with V_{Gm}. As the electrochemical potential reaches the bottom of the conduction band, we can observe an abrupt change of slope. As the charge accumulates in the device, the variation of the electrochemical potential becomes more difficult, due to the increase of the quantum capacitance of the system.[31] The spin-flip resonance region is easily reached with the tight double gate structure adopted here, which optimizes the electrostatic control. The considered oxide thicknesses are obtained with state-of-the-art semiconductor technology, and high-dielectric-constant oxides (the so-called high-K dielectrics) can allow even better electrostatic control. In the inset of Figure 5 we show the charge accumulated on the U and L plane. The charge shows an activation behavior in correspondence with the value of V_{Gm} for which the electrochemical potential reaches the conduction band.

Conclusion. We have demonstrated that bilayer graphene FETs, in which a ferromagnetic insulator is used as a gate dielectric, is an interesting system for spin manipulation. In particular, we have shown that a good electric control of spin

DOI: 10.1021/nl102298n | *Nano Lett.* **2010,** *10,* 4463–4469

rotation can be achieved even in a 2D system without lateral confinement, at low temperature. We show that by switching between a *direct* and a *reverse* gate polarization, we can modulate the ratio of spin-flipped transmitted carriers from more than 80% to less than 20%. Therefore, the system itself acts as a tunable spin-flipping device and offers the possibility to devise spin-FETs based on bilayer graphene, exploiting the exchange proximity interaction with a ferromagnetic insulator, instead of the rather weak intrinsic spin−orbit coupling.

Acknowledgment. P.M. and P.R. acknowledge financial support from the DFG via the Emmy Noether program. G.I. acknowledges financial support from the EC through the FP7 Nanosil NoE (Contract No. 216171) and GRAND project (Contract No. 215752), and from the ESF EUROCORES Program FoNE, through funds from CNR and the EC 6FP Programme, under project DEWINT (Contract ERAS-CT-2003-980409).

REFERENCES AND NOTES

(1) Novoselov, K. S.; Geim, A. K.; Morozov, S. V.; Jiang, D.; Zhang, Y.; Dubonos, S. V.; Grigorieva, I. V.; Firsov, A. A. *Science* **2004**, *306*, 666.
(2) Neto, A. C.; Guinea, F.; Peres, N.; Novoselov, K.; Geim, A. *Rev. Mod. Phys.* **2009**, *81*, 109.
(3) Geim, A. K.; Novoselov, K. S. *Nat. Mater.* **2007**, *6*, 183.
(4) Bai, J.; Duan, X.; Huang, Y. *Nano Lett.* **2009**, *9*, 2083–2087.
(5) Seidel, R. V.; Graham, A. P.; Kretz, J.; Rajasekharan, B.; Duesberg, G. S.; Liebau, M.; Unger, E.; Kreupl, F.; Hoenlein, W. *Nano Lett.* **2005**, *5*, 147–150.
(6) Michetti, P.; Cheli, M.; Iannaccone, G. *Appl. Phys. Lett.* **2010**, *96*, 133508.
(7) Fiori, G.; Iannaccone, G. *IEEE Electron Device Lett.* **2009**, *30*, 1096–1098.
(8) Cheli, M.; Michetti, P.; Iannaccone, G. Physical insigths on nanoscale FETs based on epitaxial graphene on SiC. *Proc. ESSERDC* **2009**, *2009*, 193−196.
(9) Cheli, M.; Michetti, P.; Iannaccone, G. *IEEE Trans. Electron Devices* **2010**, *57*, 1936−1941.
(10) Datta, S.; Das, B. *Appl. Phys. Lett.* **1990**, *56*, 665.
(11) Min, H.; Hill, J.; Sinitsyn, N.; Sahu, B.; Kleinman, L.; MacDonald, A. *Phys. Rev. B* **2006**, *74*, 165310.
(12) Huertas-Hernando, D.; Guinea, F.; Brataas, A. *Phys. Rev. B* **2006**, *74*, 155426.
(13) Tombros, N.; Jozsa, C.; Popinciuc, M.; Jonkman, H. T.; van Wees, B. *Nature* **2007**, *448*, 571–574.
(14) Jayasekera, T.; Kong, B. D.; Kim, K. W.; Buongiorno Nardelli, M. *Phys. Rev. Lett.* **2010**, *104*, 146801.
(15) Son, Y.-W.; Cohen, M.; Louie, S. *Nature* **2006**, *444*, 347.
(16) Cantele, G.; Lee, Y.-S.; Ninno, D.; Marzari, N. *Nano Lett.* **2009**, *9*, 3425–3429.
(17) Žutić, I.; Fabian, J.; Das Sarma, S. *Rev. Mod. Phys.* **2004**, *76323*, 410.
(18) Semenov, Y.; Kim, K.; Zavada, J. *Appl. Phys. Lett.* **2007**, *91*, 153105.
(19) Huegen, H.; Huertas-Hernando, D.; Brataas, A. *Phys. Rev. B* **2008**, *77*, 115406.
(20) Semenov, Y.; Zavada, J.; Kim, K. *Phys. Rev. B* **2008**, *77*, 235415.
(21) Dell'Anna, L.; Martino, A. D. *Phys. Rev. B* **2009**, *80*, 155416.
(22) Ohta, T.; Bostwick, A.; Seyller, T.; Horn, K.; Rotenberg, E. *Science* **2006**, *313*, 951–954.
(23) Castro, E.; Novoselov, K.; Morozov, S.; Peres, N.; dos Santos, J. L.; Nilsson, J.; Guinea, F.; Geim, A.; Neto, A. C. *Phys. Rev. Lett.* **2007**, *99*, 216802.
(24) Oostinga, J.; Heersche, H.; Liu, X.; Morpurgo, A.; Vandersypen, L. *Nat. Mater.* **2008**, *7*, 151.
(25) Zhang, Y.; Tang, T.-T.; Girit, C.; Hao, Z.; Martin, M. C.; Zettl, A.; Crommie, M. F.; Shen, Y. R.; Wang, F. *Nature* **2009**, *459*, 820.
(26) McCann, E. *Phys. Rev. B* **2006**, *74*, 161403–161407.
(27) Nilsson, J.; Neto, A. C.; Guinea, F.; Peres, N. *Phys. Rev. B* **2008**, *78*, No. 045405.
(28) Li, Z.; Henriksen, E.; Jiang, Z.; Hao, Z.; Martin, M.; Kim, P.; Stormer, H.; Basov, D. *Phys. Rev. Lett.* **2009**, *102*, No. 037403.
(29) Barbier, M.; Vasilopoulos, P.; Peeters, F.; Jr., J. P. *Phys. Rev. B* **2009**, *79*, 155402.
(30) Castro, E.; Peres, N.; dos Santos, J. L.; Guinea, F.; Neto, A. C. *J. Phys.: Conf. Series* **2008**, *129*, No. 012002.
(31) Cantele, G.; Lee, Y.-S.; Ninno, D.; Marzari, N. *Appl. Phys. Lett.* **1988**, *52*, 501.

DOI: 10.1021/nl102298n | *Nano Lett.* **2010,** *10,* 4463–4469